HHS Public Access

Author manuscript

Science. Author manuscript; available in PMC 2016 August 21.

Published in final edited form as:

Science. 2015 August 21; 349(6250): 873–876. doi:10.1126/science.aaa5619.

Membrane potential modulates plasma membrane phospholipid dynamics and K-Ras signaling

Yong Zhou[1], **Ching-On Wong**[1], **Kwang-jin Cho**[1], **Dharini van der Hoeven**[2], **Hong Liang**[1], **Dhananiay P. Thakur**[1], **Jialie Luo**[1], **Milos Babic**[3], **Konrad E. Zinsmaier**[3], **Michael X. Zhu**[1,4], **Hongzhen Hu**[1,4], **Kartik Venkatachalam**[1,4], and **John F. Hancock**[1,4,*]

[1]Department of Integrative Biology and Pharmacology, Medical School, University of Texas Health Science Center at Houston, Houston, TX 77030, USA

[2]Department of Diagnostic and Biomedical Sciences, Dental School, University of Texas Health Science Center at Houston, Houston, TX 77054, USA

[3]Department of Neuroscience, University of Arizona, Tucson, AZ 85721, USA

[4]Program in Cell and Regulatory Biology, University of Texas Graduate School of Biomedical Sciences, Houston, TX 77030, USA

Abstract

Plasma membrane depolarization can trigger cell proliferation, but how membrane potential influences mitogenic signaling is uncertain. Here, we show that plasma membrane depolarization induces nanoscale reorganization of phosphatidylserine and phosphatidylinositol 4,5-bisphosphate but not other anionic phospholipids. K-Ras, which is targeted to the plasma membrane by electrostatic interactions with phosphatidylserine, in turn undergoes enhanced nanoclustering. Depolarization-induced changes in phosphatidylserine and K-Ras plasma membrane organization occur in fibroblasts, excitable neuroblastoma cells, and *Drosophila* neurons in vivo and robustly amplify K-Ras–dependent mitogen-activated protein kinase (MAPK) signaling. Conversely, plasma membrane repolarization disrupts K-Ras nanoclustering and inhibits MAPK signaling. By responding to voltage-induced changes in phosphatidylserine spatiotemporal dynamics, K-Ras nanoclusters set up the plasma membrane as a biological field-effect transistor, allowing membrane potential to control the gain in mitogenic signaling circuits.

Plasma membrane (PM) potential (V_m) has been linked to cell survival and proliferation (1, 2). Dividing cells are more depolarized than quiescent cells, and oncogenically transformed cells are generally more depolarized than normal parental cells, indicating that $V_m$may be inversely coupled to pro-proliferative pathways (2). The mechanisms that might link V_m to cell proliferation are poorly characterized. Ras proteins are membrane-bound signaling proteins involved in cell differentiation, proliferation, and survival (3). The three

*Corresponding author. john.f.hancock@uth.tmc.edu.

SUPPLEMENTARY MATERIALS

www.sciencemag.org/content/349/6250/873/suppl/DC1

Materials and Methods

Figs. S1 to S16

ubiquitously expressed Ras isoforms—H-, N-, and K-Ras—assemble into spatially distinct nanoassemblies on the PM called nanoclusters (4). Nanocluster formation is essential for activation of mitogen-activated protein kinase (MAPK) signaling by Ras because activation of the protein kinase RAF on the PM is restricted to Ras.GTP (GTP, guanosine triphosphate) nanoclusters (5). Nanocluster assembly requires complex interactions between PM lipids and the Ras lipid anchors, C-terminal hypervariable regions, and G domains; with interactions between Ras basic residues and charged PM lipids being particularly relevant (6). The diffusion of lipids in model membranes and phase separation of multicomponent bilayers is responsive to electric fields (7, 8). We therefore tested whether the lateral distribution of anionic lipids in the PM is responsive to V_m and the potential consequences on Ras spatial organization.

We manipulated the V_m of baby hamster kidney (BHK) cells, measured by whole-cell patch clamping, by changing extracellular K^+ concentration (Fig. 1A). Simultaneously we quantified the nanoscale distribution of various green fluorescent protein (GFP)–labeled lipid-binding probes on the inner PM by using electron microscopy (EM) and spatial mapping (4, 9, 10). The analyses show that nanoclustering of phosphatidylserine (PS) and phosphatidylinositol 4,5-bisphosphate (PIP_2) was enhanced on PM depolarization, whereas there was no detectable change in the lateral distribution of phosphatidic acid (PA) or phosphatidylinositol 3,4,5-trisphosphate (PIP_3) (Fig. 1, B and C, and fig. S1). The enhanced clustering of PS was fast, being 80% complete within 30 s (the shortest assay time allowed by the EM technique) (Fig. 1D). PIP_2 clustering increased at a slightly slower rate (Fig. 1D). On repolarization of the PM, by switching from 100 mM [K^+] back to 5mM [K^+], nanoclustering of PS and PIP_2 reverted to control values with near identical kinetics (Fig. 1E). The PS content of the PM was unaffected by changingV_m (fig. S2). Fluorescence recovery after photo-bleaching assays of lipid spatiotemporal dynamics showed that the mobile fraction of fluorescently labeled PS and PIP_2 decreased significantly upon PM depolarization (fig. S3), consistent with the EM data. The differential effect of V_m on anionic PM lipids is concordant with observations that charged lipids respond differently to applied electric fields (7, 8, 11).

The localization and lateral distribution of K-Ras on the PM requires electrostatic interactions between a C-terminal polybasic domain and PS (9, 10, 12, 13). The electrostatic potential of the inner PM leaflet is independent of V_m, and concordantly total internal reflection fluorescence and confocal microscopy showed that K-Ras PM localization was insensitive to PM depolarization (fig. S5). However, EM spatial mapping experiments of BHK cells expressing GFP–K-RasG12V (GFP-labeled, constitutively GTP-bound K-Ras) showed that K-RasG12V peak $L(r) - r$ (L_{max}, where L represents a K function and r is radius) values correlated strongly with V_m, indicating that PM depolarization enhances K-Ras nanoclustering (Fig. 1F). The temporal dynamics of V_m-induced changes in K-RasG12V nanoclustering matched those of PS rather than PIP_2 (Fig. 1, D and E). To visualize nanocluster changes in intact cells, we used fluorescence lifetime imaging microscopy combined with fluorescence resonance energy transfer (FLIM-FRET). The fluorescence lifetime of GFP–K-RasG12V in cells coexpressing the FRET acceptor red fluorescent protein (RFP)–K-RasG12V decreased as a function of V_m (Fig. 1, G and H),

indicating increased FRET between GFP–K-RasG12V and RFP–K-RasG12V and hence increased K-Ras nanoclustering. Conversely, expression of the Kv2.1 channel, which hyperpolarizes the PM (14) (fig. S6C), largely eliminated FRET between GFP–K-RasG12V and RFP–K-RasG12V, consistent with disruption of K-Ras nanoclustering (fig. S6). Expression of a nonconducting channel mutant, Kv2.1W369CY384T (fig. S6C), had no effect on the lifetime of GFP–K-RasG12V in control FLIM experiments (fig. S6B). PM depolarization did not change concentrations of intracellular Ca^{2+} in BHK cells (fig. S7). Concordantly, we obtained identical EM and FLIM results in Ca^{2+}-free buffers containing the Ca^{2+} chelator EGTA (fig. S8). PM depolarization also enhanced the nanoclustering of GFP-tK but not GFP-tH (GFP coupled to the isolated membrane-anchoring domains of K-Ras and H-Ras, respectively) (Fig. 1, F to H, and fig. S8, D and E). Thus, K-Ras nanoclustering is sensitive to V_m through a mechanism that requires the C-terminal polybasic domain.

In excitable differentiated mouse Neuro2A (N2A) neuroblastoma cells (15), PM depolarization with high $[K^+]$ also caused a significant decrease in GFP fluorescence lifetime in GFP-tK and RFP-tK coexpressing cells (Fig. 2, A and B), indicating increased GFP-RFP FRET from increased GFP-tK clustering. Similar results were observed with full-length K-RasG12V (Fig. 2, A and B). Glutamate receptor–induced PM depolarization (15) also enhanced K-RasG12V clustering (Fig. 2C). This effect appeared unrelated to activation of phospholipase C (PLC), because pretreatment with the PLC inhibitor U73122 did not abrogate glutamate-stimulated K-Ras clustering but effectively blocked increases in intracellular concentrations of Ca^{2+} (fig. S9). Thus, glutamate-induced changes in K-Ras nanoclustering are also mediated through a change in PM voltage.

We evaluated the causality between V_m-induced changes in PS or PIP_2 distribution and K-Ras clustering by quantifying their colocalization using EM spatial mapping and integrated bivariate K functions (LBI values) (9). PM depolarization significantly and selectively enhanced the association of K-Ras with PS but not with PIP_2 (Fig. 3A and fig. S10), consistent with V_m-induced changes in the PM PS distribution being causally associated with increased K-Ras nanoclustering. We therefore evaluated K-Ras clustering in PS auxotroph (PSA-3) cells (16), which, when grown in the absence of ethanolamine, synthesize ~30% less total PS (16) and are depleted of PS in the inner PM leaflet (9, 16). EM-spatial mapping and FLIM-FRET imaging of ethanolamine-starved PSA-3 cells showed that PS depletion rendered K-Ras nanoclustering insensitive to V_m (Fig. 3, B and C).

Enhancing K-Ras.GTP nanoclustering increases activation of the RAF-MAPK cascade (5). We therefore examined the effect of V_m on K-Ras–specific MAPK signaling. Progressively reducing V_m enhanced phosphorylation of extracellular signal–regulated kinase (ERK) in K-RasG12V–expressing cells (Fig. 3D and figs. S11 and S12), consistent with the EM and FLIM results. ERK activation was nonlinearly dependent on V_m (Fig. 3D) unlike L_{max} (Fig. 1F). This is expected because the K-Ras clustered fraction (φ), which determines MAPK signaling output (5), is a nonlinear function of L_{max} (4) (fig. S13). MAPK activation increased rapidly in response to PM depolarization (<30 s), concordant with the time scale of enhanced K-Ras clustering, and recovered within 30 min of PM repolarization (fig. S14). V_m-induced activation of MAPK signaling in K-RasG12V–expressing PSA-3 cells was

abolished under conditions of PS depletion (fig. S11C). Thus, depleting cellular and PM PS levels effectively uncouples V_m from K-Ras clustering and signaling. Because the amounts of K-Ras.GTP are fixed in K-RasG12V cells, V_m regulates signal gain in the K-Ras signaling circuit by controlling the extent of K-Ras nanoclustering.

Last, we observed similar results in vivo in *Drosophila* (Fig. 4A) (17). Depolarization of intact fly brains expressing GFP-tK and RFP-tK resulted in increased GFP-RFP FRET (Fig. 4, B and C), indicating enhanced K-Ras clustering. Concordantly, depolarization of wild-type fly embryos significantly stimulated MAPK activation, whereas depolarization of *atp8b* mutant embryos (fig. S15) that lack a PM PS flippase (18, 19) had no effect on MAPK activation (Fig. 4D and fig. S16L). Lack of *atp8b* diminishes the inner PM leaflet of PS (18, 19) (fig. S16, A to K) and is thus a partial phenocopy of PS-deficient PSA-3 cells (fig. S11).

We show that PM depolarization induces rapid and substantial changes in the nanoscale organization of the anionic phospholipids, PS and PIP_2, on the inner leaflet of the PM. An important consequence of the PS reorganization is increased K-Ras nanoclustering, which enhances K-Ras–dependent MAPK signaling in nonexcitable and excitable cells, as well as intact fly embryo. Reduced PM V_m has long been associated with cell survival, proliferation, and differentiation (1, 2). Yet, no compelling mechanism has been proposed to explain the input of electrical signal to cell signaling cascades. We suggest that K-Ras nanoclusters, by responding to V_m-induced changes in PS spatiotemporal dynamics, allow the PM to act as a field-effect transistor to control the gain in Ras signaling circuits. Neuronal development, including plasticity, long-term potentiation, and memory, is strongly associated with V_m and MAPK signaling (20, 21); it is thus feasible that changes in PS-mediated K-Ras lateral segregation potentially play an important role these processes.

Supplementary Material

Refer to Web version on PubMed Central for supplementary material.

ACKNOWLEDGMENTS

This work was supported by grant RP130059 from the Cancer Prevention and Research Institute of Texas and grant R01NS081301 from NIH.

REFERENCES AND NOTES

1. Sundelacruz S, Levin M, Kaplan DL. Stem Cell Rev. 2009; 5:231–246. [PubMed: 19562527]
2. Blackiston DJ, McLaughlin KA, Levin M. Cell Cycle. 2009; 8:3527–3536. [PubMed: 19823012]
3. Hancock JF. Nat. Rev. Mol. Cell Biol. 2003; 4:373–385. [PubMed: 12728271]
4. Plowman SJ, Muncke C, Parton RG, Hancock JF. Proc. Natl. Acad. Sci. U.S.A. 2005; 102:15500–15505. [PubMed: 16223883]
5. Tian T, et al. Nat. Cell Biol. 2007; 9:905–914. [PubMed: 17618274]
6. Zhou Y, Hancock JF. Biochim. Biophys. Acta. 2015; 1853:841–849. [PubMed: 25234412]
7. O'Shea PS, Feuerstein-Thelen S, Azzi A. Biochem. J. 1984; 220:795–801. [PubMed: 6087795]
8. Groves JT, Boxer SG, McConnell HM. Proc. Natl. Acad. Sci. U.S.A. 1998; 95:935–938. [PubMed: 9448263]
9. Zhou Y, et al. Mol. Cell. Biol. 2014; 34:862–876. [PubMed: 24366544]
10. Ariotti N, et al. J. Cell Biol. 2014; 204:777–792. [PubMed: 24567358]

11. Starke-Peterkovic T, Clarke RJ. Eur. Biophys. J. 2009; 39:103–110. [PubMed: 19132364]
12. Yeung T, et al. Science. 2008; 319:210–213. [PubMed: 18187657]
13. Cho KJ, et al. J. Biol. Chem. 2012; 287:43573–43584. [PubMed: 23124205]
14. Park KS, Mohapatra DP, Misonou H, Trimmer JS. Science. 2006; 313:976–979. [PubMed: 16917065]
15. Van der Valk JB, Vijverberg HP. Eur. J. Pharmacol. 1990; 185:99–102. [PubMed: 1699769]
16. Lee S, et al. Genes Cells. 2012; 17:728–736. [PubMed: 22747682]
17. Brand AH, Perrimon N. Development. 1993; 118:401–415. [PubMed: 8223268]
18. Ha TS, Xia R, Zhang H, Jin X, Smith DP. Proc. Natl. Acad. Sci. U.S.A. 2014; 111:7831–7836. [PubMed: 24821794]
19. Paulusma CC, et al. Hepatology. 2008; 47:268–278. [PubMed: 17948906]
20. Impey S, Obrietan K, Storm DR. Neuron. 1999; 23:11–14. [PubMed: 10402188]
21. Kelleher RJ 3rd, Govindarajan A, Jung HY, Kang H, Tonegawa S. Cell. 2004; 116:467–479. [PubMed: 15016380]

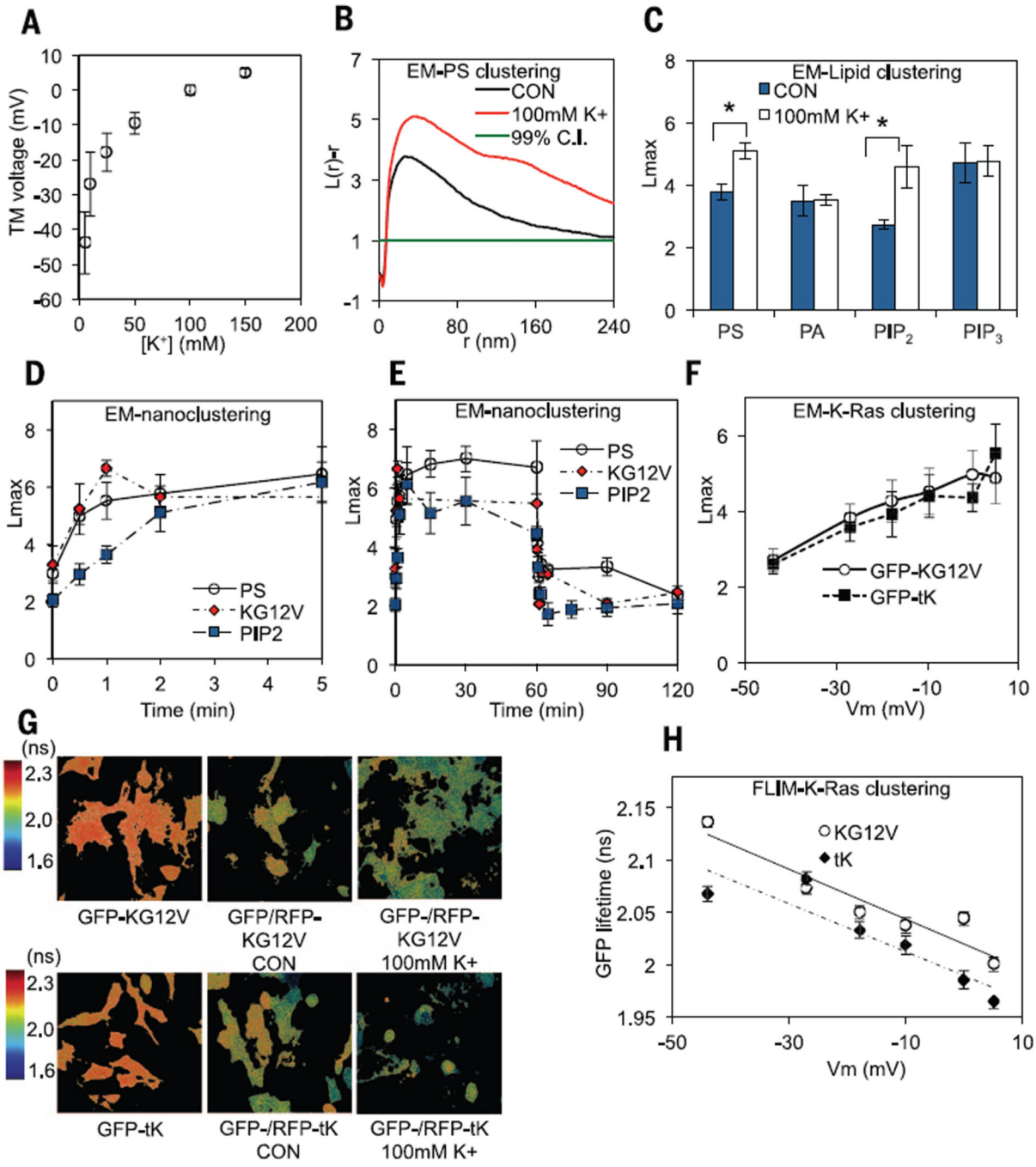

Fig. 1. PM depolarization enhances nanoclustering of lipids and K-Ras

(**A**) Whole-cell patch clamping of BHK cells to measure V_m in isotonic buffers containing different [K^+]. (**B**) Weighted mean K functions shown as $L(r) - r$ for a PS lipid probe ($n \geq 8$) in control (CON) and depolarized BHK cells. $L(r) - r$ values >99% confidence interval (C.I.) for a random pattern indicate clustering. Depolarization (100mM [K^+]) significantly increased PS clustering ($P < 0.001$, bootstrap test). (**C**) Peak $L(r) - r$ values, L_{max}, derived from curves as in (B), quantify the extent of nanoclustering of lipid probes for PS, PIP_2, PA, or PIP_3 in control and depolarized (100 mM [K^+]) BHK cells. (**D**) Short time course

(<5min) of changes in L_{max} values for PS, PIP_2, and GFP–K-RasG12V (KG12V) in BHK cells depolarized with 100 mM [K^+] at t = 0 min. (**E**) Time course of depolarization (5 to 100 mM [K^+] at t = 0 min) and repolarization (100 to 5 mM [K^+] at t = 60min), changes in L_{max} for PS, PIP2, and K-RasG12V. (**F**) Dependence of GFP–K-RasG12V or GFP-tK clustering, quantified as L_{max} values, on V_m varied as in (A). (**G**) FLIM images (GFP) of cells expressing GFP/RFP–K-RasG12V and GFP/RFP-tK FRET pairs. (**H**) Fluorescence lifetime of GFP–K-RasG12V or GFP-tK in cells expressing the cognate RFP-FRET pair plotted against V_m. Each point is the mean (±SEM) GFP lifetime measured in >60 individual cells. Significant differences (*P < 0.001) were evaluated by using one-way analysis of variance (ANOVA). Error bars in all panels represent SEM.

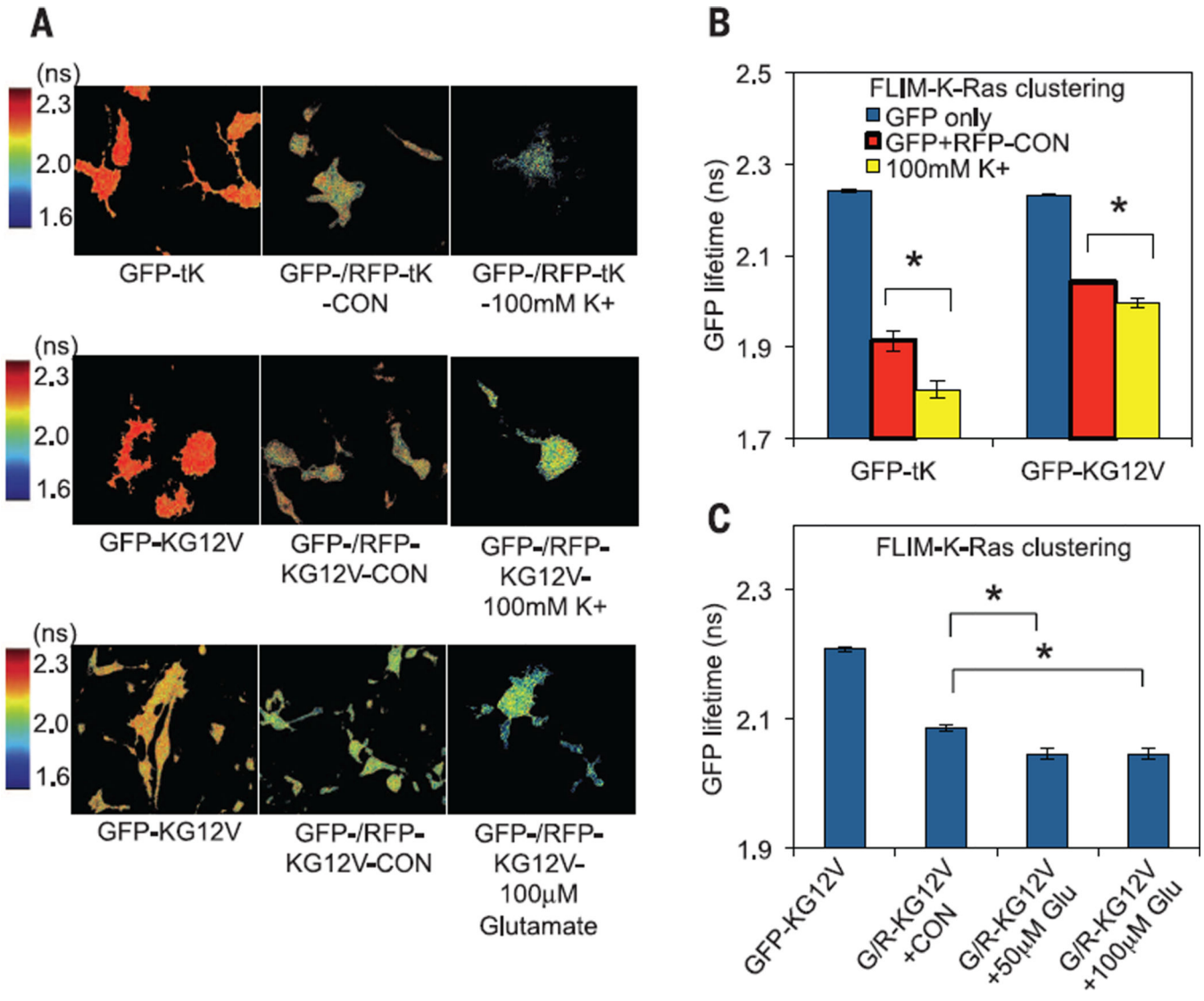

Fig. 2. Plasma membrane depolarization enhances K-Ras nanoclustering in mouse neuroblastoma cells

(**A**) FLIM images of differentiated N2A cells expressing the FRET pairs: RFP/GFP-tK or RFP/GFP–K-RasG12V (GFP-KG12V and depolarized with 100 mM [K^+] or 50 to 100 μM glutamate (Glu). (**B** and **C**) Quantification of fluorescence lifetime of GFP–K-RasG12V or GFP-tK in N2A cells expressing the cognate RFP-FRET pair treated as in (A). Each data point is the mean (±SEM) GFP lifetime measured in >60 individual cells. Significant differences (*$P < 0.01$) were evaluated by using one-way ANOVA.

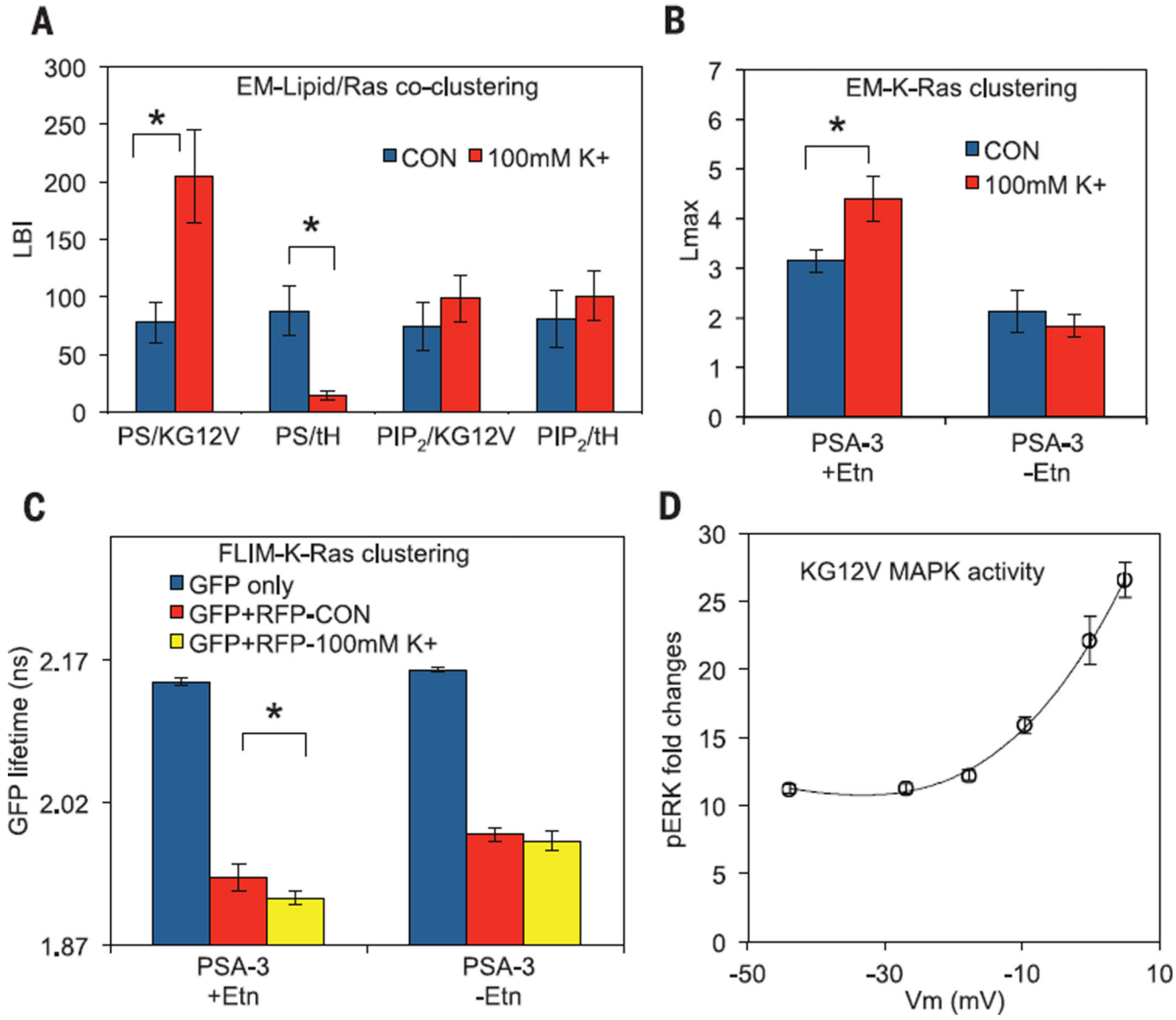

Fig. 3. PS mediates V_m-induced changes in K-Ras nanoclustering and signaling

(**A**) PM sheets from BHK cells expressing RFP–K-RasG12V, and a GFP-tagged lipid-binding probe for PS or PIP_2, were labeled with anti-GFP-6nm gold and anti-RFP-2nm gold and visualized by EM. Bivariate K functions (summarized as LBI values) were used to quantify the colocalization of PS or PIP_2 with GFP–K-RasG12V and GFP-tH nanoclusters. Statistical significance was evaluated in Mann-Whitney tests (*$P < 0.05$). Additional lipid reorganization results are shown in fig. S10E. (**B**) Univariate EM-spatial mapping of PM sheets prepared from PSA-3 cells expressing GFP–K-RasG12V and grown with or without ethanolamine (±Etn). (**C**) FLIM imaging of PSA-3 cells expressing GFP–K-RasG12V or coexpressing RFP–K-RasG12V and grown ±Etn. (**D**) MAPK activation in K-RasG12V–transformed BHK cells (and wild-type cells fig. S11) measured by quantitative immunoblotting for phosphorylated ERK (pERK) after PM depolarization as in Fig. 1A.

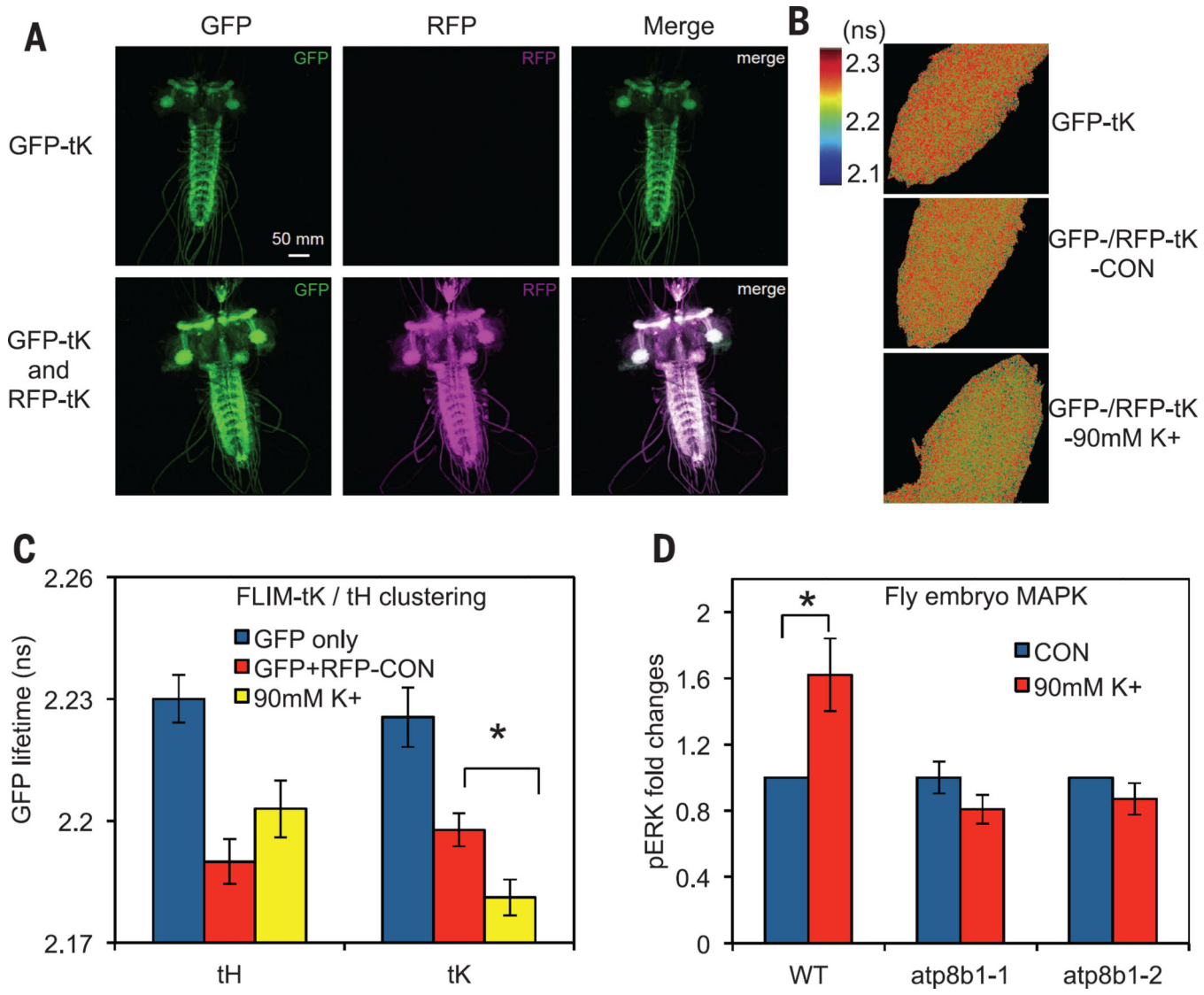

Fig. 4. Enhanced K-Ras clustering and MAPK signaling in intact fly embryo after PM depolarization

(**A**) Confocal images of flies expressing GFP-tK, or coexpressing GFP-tK and RFP-tK, from a neuronal-specific promoter. (**B**) FLIM imaging of brains from flies in (A) in control buffer and after depolarization with high [K^+]. (**C**) Quantification of fluorescence lifetime of GFP-tK in fly brains expressing the cognate RFP-FRET pair treated as in (B); results are mean (±SEM, n = 9). High [K^+] had no effect on the fluorescence lifetime of GFP-tH in fly brains expressing GFP-tH and RFP-tH. (**D**) Fly embryos from wild-type (WT) and mutant *atp8b* flies incubated in 5 or 90 mM K^+ for 15 min and then immunoblotted for pERK. Results are quantified as mean ± SEM (n =3).